Received: 4 June 2019 | Revised: 23 November 2019 | Accepted: 15 December 2019

DOI: 10.1002/mrm.28165

FULL PAPER

Magnetic Resonance in Medicine

Single-shot EPI for ASL-CMR

Ahsan Javed | **Krishna S. Nayak**

Ming Hsieh Department of Electrical and Computer Engineering, University of Southern California, Los Angeles, California

Correspondence
Ahsan Javed, 3740 McClintock Avenue, EEB 400, University of Southern California, Los Angeles, CA 90089-2564.
Email: ahsan.javed@nih.gov

Funding information
Grant Sponsor: National Institutes of Health R01-HL130494

Purpose: To evaluate single-shot echo planar imaging (SS-EPI), as an alternative to snapshot balanced steady state free precession (bSSFP) imaging, for arterial-spin-labeled cardiac MR (ASL-CMR). This study presents a practical implementation SS-EPI tailored to the needs of ASL-CMR at 3T and demonstrates sequential multi-slice ASL with no increase in scan time.

Methods: Reduced field of view SS-EPI was performed using a 2DRF pulse. A spin-echo was used with crushers optimized to maximize blood suppression and minimize myocardial signal loss, based on experiments in 4 healthy volunteers. SS-EPI was evaluated against the widely used bSSFP reference method in single-slice ASL-CMR in 4 healthy volunteers, during both systole and diastole. Sequential multi-slice ASL-CMR with SS-EPI was demonstrated during diastole (3 slices: basal, mid, and apical short-axis) and during systole (2 slices: mid and apical short-axis), in 3 volunteers.

Results: Global myocardial perfusion for diastolic SS-EPI (1.66 ± 0.73 mL/g/min) and systolic SS-EPI (1.50 ± 0.36 mL/g/min) were found to be statistically equivalent (2 one-sided test with a difference of 0.4 mL/g/min) to diastolic bSSFP (duration of 1 cardiac cycle, 1.60 ± 0.80 mL/g/min) with *P*-values of 0.022 and 0.031, respectively. Global myocardial perfusion for sequential multi-slice experiments was 1.64 ± 0.47, 1.34 ± 0.29, and 1.88 ± 0.58 for basal, mid, and apical SAX slices during diastole and was 1.61 ± 0.35, and 1.66 ± 0.49 for mid and apical slice during systole. These values are comparable to published ASL-CMR and positron emission tomography studies.

Conclusion: SS-EPI is a promising alternative to bSSFP imaging for ASL-CMR and can potentially improve the spatial coverage of ASL-CMR by 3-fold during diastole and 2-fold during systole, without increasing scan time.

KEYWORDS

arterial spin labeling, inner volume imaging, myocardial perfusion, reduced field of view imaging, single-shot echo planar imaging

1 | INTRODUCTION

Arterial spin labeled cardiac MR (ASL-CMR) is a noncontrast technique that can assess myocardial perfusion (MP) and detect angiographically significant coronary artery disease (CAD).[1,2] Approximately 17.6 million Americans suffer from CAD,[3] and it is responsible for more than 350 thousand deaths in the United States each year.[4] Coronary angiography is the clinical gold standard for diagnosis of CAD. However, it is an invasive technique, exposes patients to

ionizing radiation, has high risk of complications, and cannot be used repeatedly. Single photon emission computed tomography and CMR first pass perfusion are noninvasive alternatives that can measure regional MP and MP reserve (using vasodilation) for diagnosis of CAD. Single photon emission computed tomography also exposes patients to ionizing radiation, and CMR first pass techniques requires the use of contrast agents that are contraindicated for patients with kidney disease.[5] Patients with chronic kidney disease and end-stage renal disease are at a higher risk for CAD and rates of end-stage renal disease are rising annually at 3-4% in the United States[6,7] and 7% worldwide. There is a growing need for a safe and repeatable method to assess CAD. Cardiac ASL can be beneficial in this regard, because it uses no ionizing radiation or contrast agents, it provides a quantitative MP measurement, and it can be used repeatedly or even continuously to measure MP without any risk to the patients.[2]

Current ASL-CMR stress test protocols provide only single-slice coverage which is insufficient for clinical imaging.[8] The American Heart Association guidelines recommend at least 3 short-axis (SAX) slices to assess all coronary artery territories.[9] Spatial coverage can be increased using either sequential or simultaneous multi-slice (SMS) imaging. Currently, both of these techniques are not feasible with snapshot balanced steady state free precession (bSSFP) imaging, the most common ASL-CMR acquisition. Sequential multi-slice imaging with bSSFP would require an imaging window of ~600 ms, which is much longer than stable diastole. SMS imaging with bSSFP imaging has many unresolved artifacts due to off-resonance and imprecise excitation. These artifacts can corrupt the ASL signal.[10,11]

In this work, we revisit single-shot echo-planar imaging (SS-EPI) for ASL-CMR. SS-EPI was the earliest imaging scheme proposed for ASL-CMR at 1.5T by Poncelet et al[12] and remains a promising alternative to snapshot bSSFP. With modern high-performance gradients, it has the potential to reduce the imaging window (from ~200 ms) to ~55 ms without compromising spatial resolution. The short imaging window can potentially enable sequential multi-slice imaging to improve spatial coverage. In recent years, SS-EPI has been successfully applied to cardiac diffusion tensor imaging, which, like ASL, is a low signal-to-noise ratio (SNR) and highly motion-sensitive technique.[13,14] In cardiac diffusion tensor imaging SS-EPI achieved in-plane resolution of 2.7 × 2.7 mm for both single-slice and SMS systolic imaging with inner-volume excitation,[15] readout durations of 11-14 ms and using parallel imaging with partial k-space. In this study, we make 3 modifications to these published SS-EPI implementations that are relevant to ASL. First, ASL benefits from sequential multi-slice imaging which requires a change in the implementation of inner-volume imaging. Second, ASL is sensitive to changes in myocardial signal intensity, requiring systematic study of the velocity-selective effects of crusher gradients on both myocardial and blood pool signal. Third, ASL requires higher in-plane spatial resolution to minimize partial voluming effects from the blood pool that can bias MP measurements.

In this work, we present a practical implementation SS-EPI tailored to the needs of ASL. We achieve a reduced field of view (rFOV) using with 2DRF excitation, in a way that is compatible with sequential multi-slice imaging. We analyze the velocity-selective effect specific to cardiac imaging and determine the SS-EPI settings that maximizes temporal SNR (TSNR) for both systolic and diastolic imaging. Optimized SS-EPI is then compared with bSSFP for single-slice ASL-CMR. We also demonstrate sequential multi-slice ASL-CMR with no increase in scan time.

2 | METHODS

2.1 | Pulse sequence

A product EPI pulse sequence (GE Healthcare, Waukesha, WI) was modified to include a novel 2D radiofrequency (2DRF) excitation that achieves reduced FOV (rFOV) SS-EPI,[16,17] as shown in Figure 1. The 2DRF was designed with a fly-back echo planar trajectory in excitation k-space to avoid Nyquist ghosts along the slice-select axis due to gradient and timing imperfections. Oscillating and blipped gradients were played on the phase-encoding axis and slice-select axis, respectively. Selection along the phase-encode direction is controlled by the sub-pulses. Each sub-pulse was designed using the Shinnar Le-Roux algorithm[18] with a time bandwidth (BW) product of 10, 1% passband ripple, 1% stopband ripple, 8-cm passband, 14 cm phase-encode FOV, and 35 dB attenuation outside the phase-encode FOV. Selection along the slice-select direction is controlled by the envelope by which the 23 sub pulses are scaled. This envelope was also designed using the Shinnar Le-Roux algorithm with a time BW of 2.2. The sub pulse spacing was chosen to shift the fat excitation by at least 30 mm. This fat signal was subsequently suppressed by only refocusing a 20-mm slice. The overall pulse duration was minimized by (1) using maximum gradient slew rate for fly-back gradients, and (2) using the variable rate selective excitation (VERSE) algorithm[19,20] and playing RF during gradient ramps. These specifications were heuristically optimized, and in our experience, provide consistent image quality.

Figure 2 illustrates the simulated RF pulse profiles for excitation and refocusing. To enable sequential multi-slice imaging slice replicas were kept 10 cm away which ensures that only 1 slice within the left ventricle (LV) will be excited with each excitation. Based on simulation, the pulse profile in the phase-encode direction has an 8-cm passband and <1%

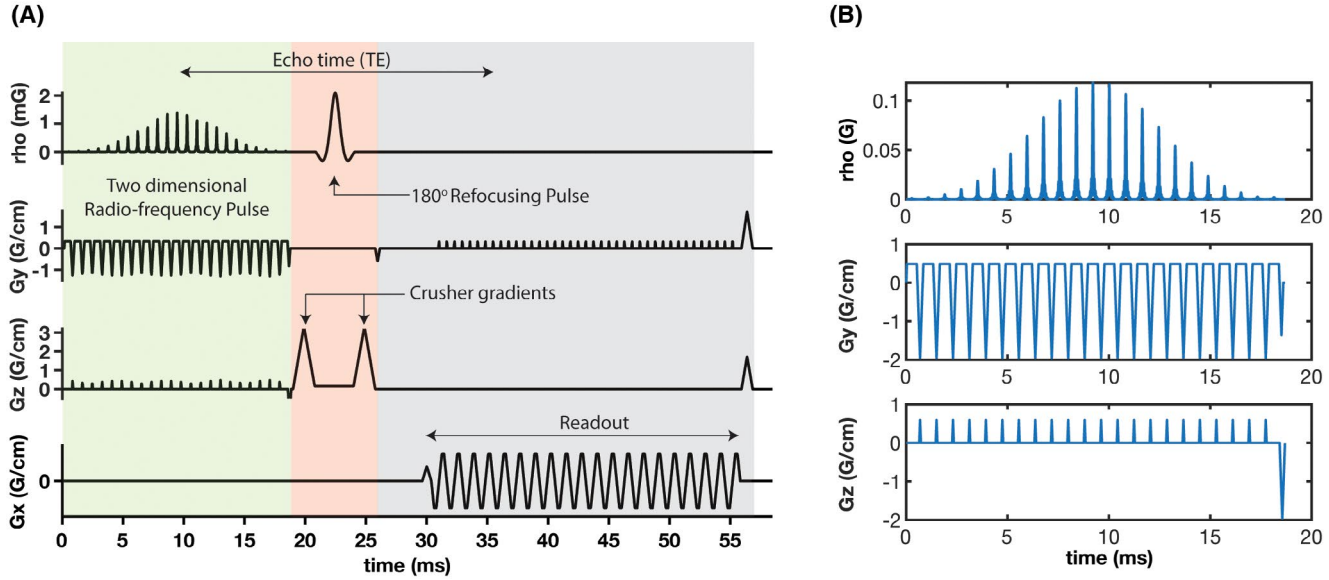

FIGURE 1 A, SS-EPI pulse sequence is comprised of a 90° spectral-spatial 2DRF excitation pulse (green), 1D selective 180° spin echo pulse (pink) with crusher gradients that provide blood suppression, and a single-shot partial Fourier echo-planar readout (gray). B, The 2DRF pulse contains 23 subpulses. Selection along the phase-encode direction is controlled by the subpulse shape and Gy gradient (oscillating). A fly-back trajectory was used to avoid ghosting due to gradient and timing imperfections. Selection along slice direction is controlled by the RF envelope and Gz gradient (blipped). The individual subpulses and the envelope were both designed using the Shinnar Le-Roux algorithm[18]

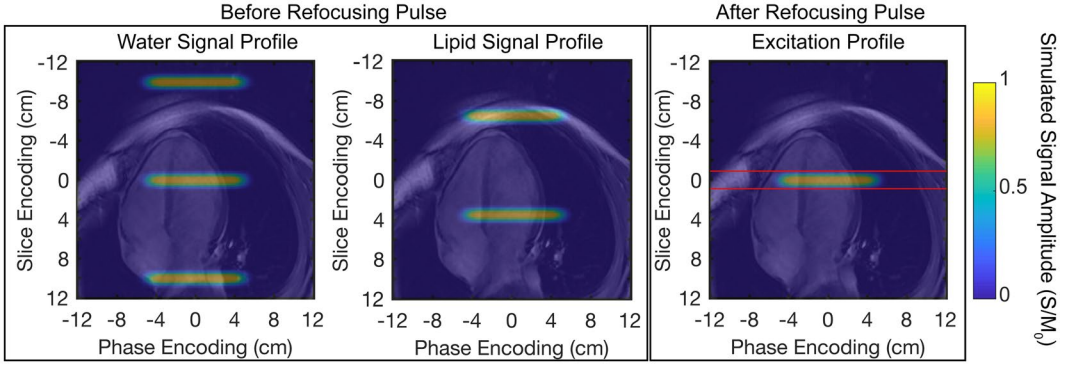

FIGURE 2 Simulated water and lipid signal profiles overlaid on a diastolic 4-chamber image to scale. (Left) Water signal for 2DRF pulse. (Center) Lipid signal for 2DRF pulse. (Right) Excitation profile after the slab-selective 180° refocusing pulse. Red lines represent the FWHM of the 180° refocusing pulse. Simulated signal amplitude (S/M_o) is depicted in color. Lipid excitation is shifted by ~3.5 cm relative to water, moving it outside the passband of the refocusing pulse. Replicas for both water and lipid signal are 10 cm apart in the slice encoding direction. Only the water signal at the desired slice location is refocused by the 180° pulse

signal in the stopband. Fat excitation is shifted by 35 mm and not included in the refocusing slab.

2.2 | Optimization of velocity suppression

The proposed SS-EPI sequence provides inherent flow suppression. Specifically, the crusher gradients around the 180-SE pulse, shown in Figure 1, create velocity-dependent phase. When intravoxel velocity is heterogenous, this produces saturation. This mechanism has been exploited in velocity-selective ASL[21] and motion-sensitized driven equilibrium flow suppression pulses.[22] A common approximation is that uniform velocity distributions [0, V_{max}] with peak velocities V_{max} above $V_c = \pi/2\gamma M_1$ are suppressed, where gamma is the gyromagnetic ratio and M_1 is the 1st moment of crusher gradients. A low V_c is expected to suppress the LV blood pool signal, which reduces flow artifacts, and partial voluming effects for myocardial imaging. However, this can potentially reduce the myocardial signal. The tradeoff between myocardial signal loss and blood suppression was experimentally characterized in 4 volunteers for both systolic and diastolic cardiac phases, leading to a V_c of 25 cm/s in systole and 12 cm/s in diastole, as

shown in Supporting Figure S1. Details can be found in the Supporting Information, which is available online.

2.3 | Evaluation of geometric distortion

SS-EPI is susceptible to geometric distortion artifacts along the phase-encode direction due to off-resonance.[23] This presents a well-known challenge in myocardial imaging at 3T.[24] These artifacts can degrade image quality and cause signal loss especially in the lateral and inferior LV walls due to proximity to the lungs and draining coronary veins.[25] The artifact can persist elsewhere if there are implanted metal such as valve clips.[26] Rotating the scan plane will change the direction of geometric distortion and improve image quality. Four to 6 scan plane rotations (30° increment) were acquired for each subject. The final rotation angle was selected by the scan operator by visual inspection, based on uniformity of LV myocardium thickness, and on least amount of signal loss. This process was repeated for both systole and diastole to account for potential differences in off-resonance with cardiac phase.

2.4 | ASL data collection

Double gated flow alternating inversion recovery (DG-FAIR) ASL[12,27] was performed in SAX slices, shown in Figure 3. Adiabatic hyperbolic-secant pulses were used for labeling. SS-EPI and bSSFP were used for imaging, in separate scans. Labeling and imaging were performed during end-systole for systolic scans and mid-diastole for diastolic scans. A gated cine bSSFP scan was used to visually determine stable systolic and diastolic phases. All acquisitions were cardiac gated using a fingertip plethysmograph.

DG-FAIR experiments were performed with post labeling delay (PLD) of 1RR and 2RR (RR is the duration of 1 cardiac cycle). PLD was defined as the duration from center of labeling pulse to center of the imaging window, such that measured MP reflects average perfusion during PLD period, as shown in Figure 1. This enables pairwise comparisons with 1 independent variable, for example 1RR bSSFP can be directly compared with 2RR bSSFP, and 2RR bSSFP can be directly compared with 2RR SS-EPI. SS-EPI benefits from PLDs > 1RR because at 1RR there is inadequate contrast in control and label images to perform LV segmentation. Direct

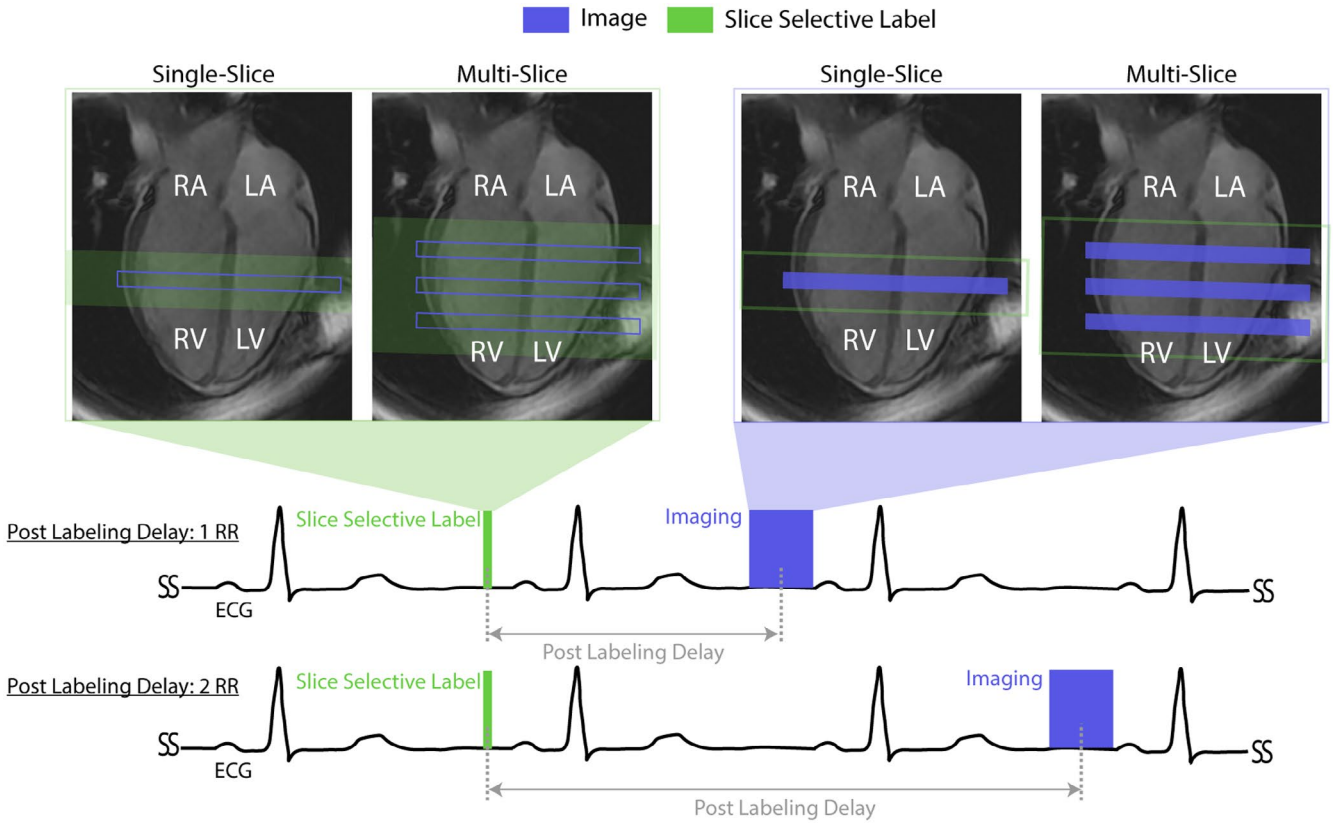

FIGURE 3 Graphic prescription and sequence timing. (Bottom) timing of diastolic DG-FAIR ASL with PLD of 1RR, and 2RR. (Top) graphic prescription performed using a 4-chamber cine. The imaging slices (purple) are SAX slices at mid-diastole. Images were acquired at mid SAX for single-slice experiments and at basal, mid, and apical SAX for diastolic multi-slice experiments. The labeling slab (green) for control labeling covers the imaging slices for both single- and multi-slice experiments. Labeling slab of 30 mm was used for single slice and 70 mm was used for diastolic multi-slice experiments. Prescription for systolic experiments was similar, but was done on an end-systole 4-chamber view. For systolic multi-slice experiments, only mid, and apical SAX slices were acquired, using a 50-mm labeling slab

subtraction of control and label images is not feasible in human ASL-CMR due to variations in breath-hold position. Therefore, some blood-myocardium contrast is required to facilitate image-to-image registration. In SS-EPI with PLD of 1RR, both blood pool (due to velocity selective suppression) and myocardium are near zero and difficult to distinguish. SS-EPI requires a PLD > 1RR to provide blood-myocardium contrast sufficient for reliable LV segmentation and/or registration of control and label images for ASL analysis.

SS-EPI acquisition parameters: FOV 28 × 14 cm, echo time/repetition time 31.3 ms/55 ms, flip angle 90º, matrix size 128 × 64, partial Fourier factor 5/8th, and readout time = 25 ms. bSSFP acquisition parameters: FOV 18-24 cm, slice thickness 1 cm, echo time/repetition time 1.3 ms/3.1 ms, flip angle 50º, matrix size 96 × 96, GeneRalized Autocalibrating Partial Parallel Acquisition with 24 auto-calibration lines, and effective acceleration R = 1.6.

Six-pairs of control and labelled images were acquired for each DG-FAIR scan using slice selective and nonselective labeling, respectively. Each pair of images was acquired during a 10-12 s breath-hold to avoid mis-registration. A delay of 6 s between each image acquisition allowed complete T1 recovery. A separate baseline image (i.e., an image without any preparation pulse), noise image, and an image with minimum possible PLD was also acquired. These images were used to estimate coil sensitivity, noise covariance, and for quantification, respectively. Sensitivity maps for SS-EPI were acquired using the vendor's calibration scan.

All experiments were performed on a clinical 3T scanner (GE Signa Excite HDxT, Waukesha, WI) with 8-channel cardiac receiver coil. Four healthy volunteers (1M/3F; age, 27-36 years) were recruited for this study. The imaging protocol was approved by our institutions review board and informed consent was obtained from all the volunteers. In all subjects, we performed single-slice DG-FAIR SS-EPI (PLD 2RR) and single-slice DG-FAIR bSSFP (PLD, 1RR and 2RR), during both stable systole and diastole. We also performed sequential multi-slice DG-FAIR SS-EPI. Basal, mid, and apical SAX slices were acquired for diastolic imaging. Mid and apical SAX slices were acquired for systolic imaging. The order of slice acquisition was base to apex. The labeling slab thickness was 30 mm, 50 mm, and 70 mm for the single, multi-slice systolic, and multi-slice diastolic experiments, respectively.

2.5 | ASL data analysis

Standard SS-EPI distortion correction and reconstruction were performed using the Orchestra reconstruction toolbox (GE Healthcare, Waukesha, WI). This included linear phase correction and gridding of ramp-sampled data. bSSFP images were reconstructed using a custom implementation of GeneRalized Autocalibrating Partial Parallel Acquisition.[28] In both settings, channel images were combined using optimal B_1 combination.[29] Per pixel SNR maps were computed using the pseudo-replica method.[30] One pair of control and label images were manually segmented and the masks were propagated to all other images in the series using image registration[31] implemented using Advanced Normalization Tools.[32] Spatial filtering was performed to calculate regional signal intensities which were then used for MP quantification.[33] MP for both single-slice and multi-slice data was calculated in the same way.

MP was calculated using the interpolated signal difference (ΔM) between control and label T_1 curves as described by Poncelet et al.[12] and Do et al,[27] in units of mL-blood/g-tissue/min. T1 curves for control and label images were fitted using established 3 parameter model for T1 mapping.[34] ΔM between control and label T1 curves was estimated at the average inversion time (TI_{avg}) of control and label images. MP was then calculated using the following equation:

$$f = \frac{\Delta M}{\alpha M_0 TI_{avg} e^{-TI_{avg}/T_{1blood}}} \quad (1)$$

derived from Buxton's general kinetic model,[35] where α is inversion efficiency, M_0 is equilibrium magnetization, f is MP, TI_{avg} is mean inversion time of control and label images, and T_{1blood} is the T_1 of arterial blood (1950 ms at 3T based on Weingärtner et al).[36] α was estimated with an image acquired immediately after a nonselective inversion (TI of ~160 ms) and a baseline image (representing complete recovery, TI of 9500 ms). In multi-slice studies, the slice specific TI_{avg} was used during MP quantification. Mis-triggered images were visually identified and rejected. Physiological noise (PN) is calculated as the standard error in perfusion measurements, as described by Poncelet et al,[12] in units of mL-blood/g-tissue/min. MP measurement quality was evaluated using TSNR (TSNR = MP divided PN).

Segmental analysis was performed in the mid SAX slices for single-slice experiments, using the standard American Heart Association model.[37] Global analysis was performed for multi-slice experiments. Statistical equivalence of MP measurements between different ASL-CMR techniques was established using a 2 one-sided test (TOST)[38] at a difference of 0.4 mL/g/min. Statistical differences in TSNR between techniques was established using a paired t-test.

3 | RESULTS

3.1 | Data quality

Figure 4 illustrates the impact of prescription angle on geometric distortion in SS-EPI images. As expected, the

geometric distortion stemming from off-resonance was always along the phase-encode direction. Geometric distortion was most severe in the lateral wall, which is adjacent to the lungs and draining veins.[25] Changing the rotation angle affected the amount of signal loss, and uniformity of the myocardium. In this example, rotation angle of 0° was selected because it provided images with most uniform LV thickness and least amount of signal loss upon visual inspection. The rotation angle scout scan was completed in under 3 min for all subjects.

Figure 5 contains representative control and label images for SS-EPI and bSSFP. These illustrate typical image quality, geometric distortion artifacts, and blood suppression. Average myocardial SNR for SS-EPI (diastole: 61.1 ± 9.3 and systole: 67 ± 7.9) was higher than bSSFP (diastole: 34.8 ± 6.8 and systole: 36.1 ± 6.6). bSSFP images acquired

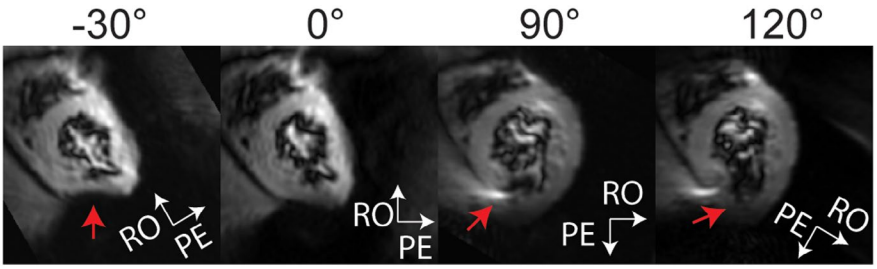

FIGURE 4 Illustration of SS-EPI geometric distortion from 1 healthy volunteer, and its dependence on graphic prescription. Baseline images are shown with different in-plane rotations (RO: readout, and PE: phase-encode directions are labeled). As expected, the geometric distortion stemming from off-resonance is always along the phase-encode direction. Arrows (red) show most severe geometric distortion in the lateral wall, which is adjacent to the lungs and draining veins.[25] Rotation angle that produced LV myocardium with least amount of signal loss, and most uniform thickness was selected. Based on these criteria, in the above example rotation angle of 0° was selected

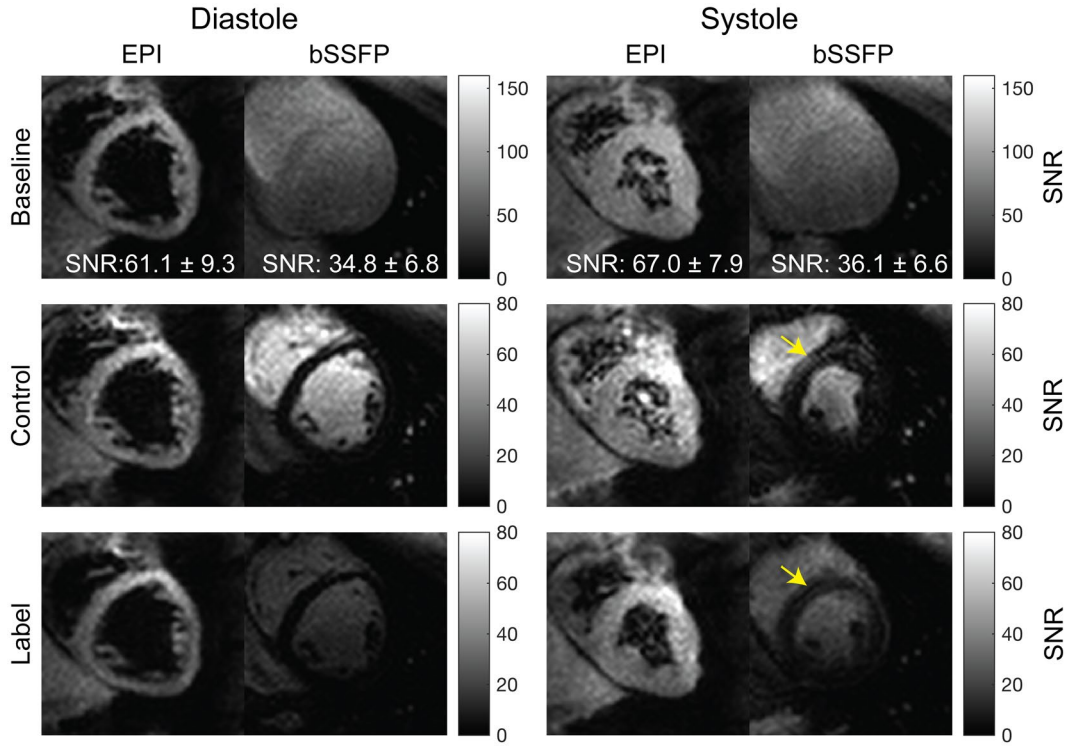

FIGURE 5 Representative SS-EPI and bSSFP images from 1 healthy volunteer: (top) baseline, (center) control, and (bottom) labeled images, during (left) diastole and (right) systole. The images are cropped to 12 × 12 cm. Colormap represents pixel values in SNR units. Baseline myocardial SNR is presented as mean ± standard deviation across 4 subjects. bSSFP images were acquired with 1RR PLD, as this is the reference method. SS-EPI images were acquired with 2RR postlabeling delay to provide adequate contrast for LV segmentation. Systolic bSSFP images show motion artifacts (yellow arrow), likely due to the long acquisition window. SS-EPI images show −20 dB diastolic and −7 dB systolic blood suppression, approximately twofold higher baseline SNR, and stronger blood-myocardium contrast, compared with bSSFP. SS-EPI images show the typical geometric distortions in a mid-SAX slice due to off-resonance

during systole showed motion artifacts (see yellow arrows), likely due to long acquisition window (192 ms), which was greater than stable end-systole. These artifacts were not observed in SS-EPI images. SS-EPI images showed −20 dB diastolic and −7 dB systolic blood suppression, which resulted in higher blood myocardium contrast than bSSFP images.

3.2 | Validation

Figure 6 summarizes validation experiments comparing DG-FAIR SS-EPI against bSSFP. Six of 24 and 2 of 24 control and label pairs were rejected for diastolic and systolic SS-EPI, respectively, due to mis-triggering. Error bars for MP and TSNR represent the standard deviation across subjects (e.g., inter-subject variability). These values are also presented in Table 1. Global MP for diastolic SS-EPI (1.67 ± 0.72 mL/g/min) and systolic SS-EPI (1.50 ± 0.36 mL/g/min) were found to be statistically equivalent to diastolic bSSFP (1RR: 1.59 ± 0.80 mL/g/min) based on TOST with *P*-values of 0.022 and 0.031, respectively. MP values for diastolic SS-EPI, systolic SS-EPI and diastolic bSSFP were comparable to previous ASL-CMR studies[27] with diastolic 1RR bSSFP, but were slightly higher than previous positron emission tomography[39] and first pass CMR[40] studies. CMR first pass studies[41] have shown that

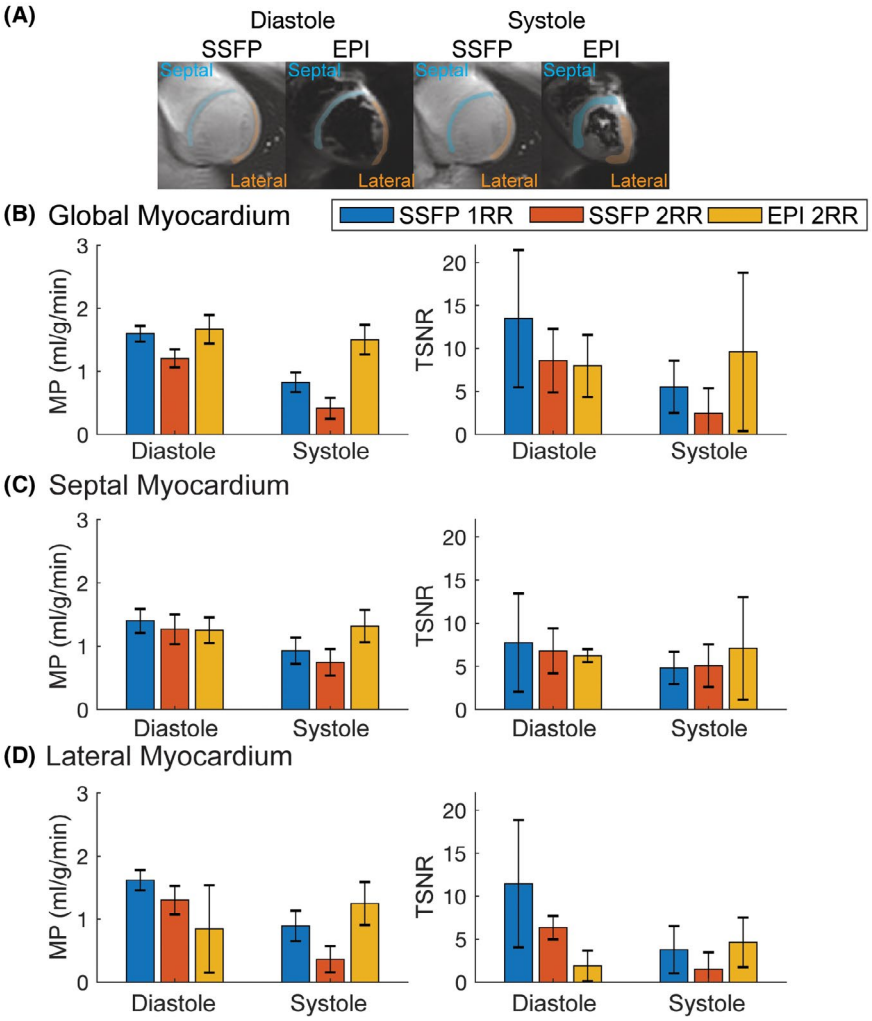

FIGURE 6 Comparison of SS-EPI and bSSFP ASL in mid SAX slices of 4 healthy volunteers. A, LV regions of interest. MP and TSNR measurements are summarized for (B) global (C) septal, and (D) lateral myocadium. Globally, diastolic and systolic SS-EPI were statistically equivalent to diastolic bSSFP 1RR with *P*-values of 0.022 and 0.031 using the TOST procedure at a MP difference of 0.4 mL/g/min. In septal regions, MP measured with diastolic SS-EPI, systolic SS-EPI, and diastolic bSSFP 2RR were equivalent to diastolic bSSFP 1RR with *P*-values 0.015, 0.012, and 0.019, respectively. In lateral regions, MP in systolic SS-EPI and diastolic bSSFP 1RR were equivalent to diastolic bSSFP 2RR with *P*-value of 0.004, and 0.043. TSNR in diastolic SS-EPI, systolic bSSFP 1RR, and bSSFP 2RR was significantly lower compared with diastolic bSSFP 1RR with *P*-values of 0.017, 0.039, and 0.022. Error bars for MP were calculated by averaging PN across subjects and demonstrate measurement variability (average intra-subject variability). Error bars for TSNR were calculated as standard deviation in TSNR across subjects (inter-subject variability)

resting MP in systole and diastole should be equivalent. In systole, global MP of bSSFP (1RR: 0.83 ± 0.51 mL/g/min, and 2RR: 0.41 ± 0.52 mL/g/min) was lower than SS-EPI (1.50 ± 0.36 mL/g/min).

Global TSNR was highest for diastolic bSSFP (1RR: 13.46 ± 7.98). It was similar in diastolic bSSFP (2RR: 8.59 ± 3.69), diastolic SS-EPI (7.97 ± 3.62), and systolic SS-EPI (9.59 ± 9.22). In systole, global TSNR of bSSFP (1RR: 5.54 ± 3.05, and 2RR: 2.45 ± 2.93) was lower than SS-EPI. Our sample size was too small to establish statistical significance of any differences in global TSNR.

Figure 6B,C shows MP and TSNR measured in the septal and lateral myocardium. Trends were generally similar to that of global myocardium, as shown in Table 1. However, for the lateral myocardium, only MP values from systolic SS-EPI (1.24 ± 0.53 mL/g/min) and diastolic bSSFP (2RR: 1.30 ± 0.80 mL/g/min) were found to be statistically equivalent, based on TOST with a *P*-value of 0.004. Surprisingly, the TSNR of diastolic SS-EPI (1.89 ± 1.79) was significantly lower than diastolic 1RR bSSFP (11.45 ± 7.41), based on a t-test with a *P*-value of 0.017.

3.3 | Multi-slice demonstration

Figure 7 contains sequential multi-slice SS-EPI images for 3 subjects. These were all acquired in the same scan duration as a single-slice acquisition. Basal, mid, and apical mid SAX

TABLE 1 MP and TSNR in 4 healthy volunteers for a single mid SAX slice

		Global		Septal		Lateral		Per-segment	
		MP	**TSNR**	**MP**	**TSNR**	**MP**	**TSNR**	**MP**	**TSNR**
Diastole	bSSFP 1RR	1.60 ± 0.80	13.46 ± 8.0	1.40 ± 0.94	7.75 ± 5.6	1.61 ± 0.92	11.45 ± 7.4	1.64 ± 0.81	10.0 ± 5.1
	bSSFP 2RR	1.21 ± 0.87	8.59 ± 3.69	1.26 ± 0.86	6.79 ± 2.6	1.30 ± 0.80	6.36 ± 1.35	1.13 ± 0.86	5.55 ± 1.65
	SS-EPI 2RR	1.66 ± 0.73	7.97 ± 3.62	1.25 ± 0.24	6.24 ± 0.7	0.84 ± 1.33	1.89 ± 1.79	1.53 ± 0.65	4.32 ± 1.38
Systole	bSSFP 1RR	0.82 ± 0.51	5.54 ± 3.05	0.93 ± 0.50	4.81 ± 1.9	0.89 ± 0.64	3.78 ± 2.74	0.71 ± 0.13	3.37 ± 0.97
	bSSFP 2RR	0.41 ± 0.53	2.45 ± 2.93	0.74 ± 0.73	5.09 ± 2.5	0.36 ± 0.45	1.51 ± 1.96	0.67 ± 0.46	3.64 ± 1.64
	SS-EPI 2RR	1.50 ± 0.36	9.59 ± 9.22	1.31 ± 0.55	7.09 ± 5.9	1.24 ± 0.53	4.63 ± 2.88	1.53 ± 0.41	5.51 ± 3.43

Values for global, septal, and lateral myocardium within the slice are presented as mean ± standard deviation across all subjects (inter-subject variability). Per-segment measurements include all 6 segments independently. Mean per-segment values are presented as average over all subjects and segments, whereas per-segment standard deviation is computed as the standard deviation over 6-segments within each subject averaged over all subjects (intra-subject variability). Segment abbreviations (counterclockwise from right ventricular insertion point): AS = anterior septal, IS = inferior septal, IN = inferior, IL = inferior lateral, AL = anterior lateral, AN = anterior. Global = average over entire myocardium; Septal = average over AS and IS; Lateral = average over AL and IL; Per-Segment = each segment independently.

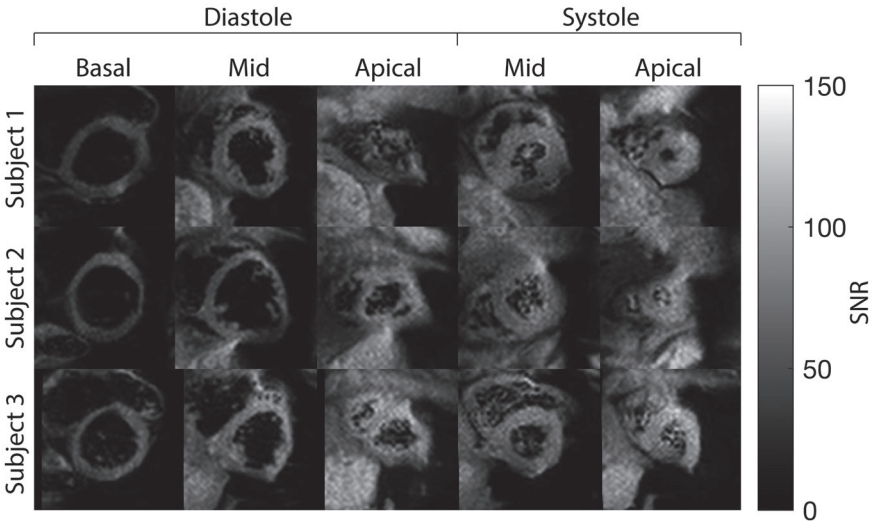

FIGURE 7 Baseline multi-slice SS-EPI images from 3 healthy volunteers. Basal, Mid, and Apical slices are shown for diastole. Mid and apical slices are shown for systole. The images are cropped to 12 × 12 cm. The SS-EPI velocity cutoff was 25 cm/s for systolic and 12 cm/s for diastolic images. Similar to single-slice SS-EPI, multi-slice SS-EPI images show −20 dB diastolic and −7 dB systolic blood suppression, higher baseline SNR, and high blood-myocardium contrast. Geometric distortion in apical slice during diastole was severe and resulted in poor image quality. Pixel intensities are shown in SNR units and were calculated using the pseudo-replica method

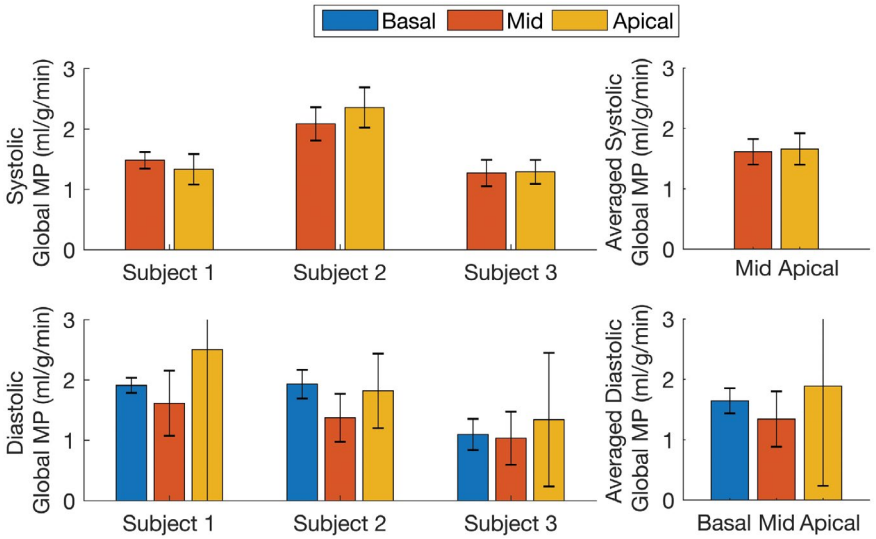

FIGURE 8 Demonstration of sequential multi-slice ASL-CMR using SS-EPI. Bar plots of global MP in basal (blue), mid (orange), and apical (yellow) slices for 3 volunteers are shown (left) for each subject, and (right) averaged. (top) Systolic global MP is shown for mid, and apical slices. (bottom) Diastolic global MP is shown for basal, mid, and apical slices. Error bars represent global PN per slice (left) global PN in each subject and (right) global PN averaged over all subjects

slices are shown for diastole whereas mid and apical slices are shown for systole. Image quality, blood suppression, and contrast between blood pool and myocardium was visually comparable to single-slice SS-EPI images. Geometric distortion in the apical slice during diastole was severe and resulted in lower image quality. This was not an issue for apical slices acquired during systole.

Figure 8 shows global MP for sequential multi-slice SS-EPI. Global MP for sequential multi-slice experiments was 1.64 ± 0.47 mL/g/min, 1.34 ± 0.29 mL/g/min, and 1.88 ± 0.58 mL/g/min for basal, mid, and apical slices, respectively, during diastole. Global MP was 1.61 ± 0.35 mL/g/min, and 1.66 ± 0.49 mL/g/min for mid, and apical slices, respectively, during systole. MP measured in all slices during both diastole and systole was comparable to previous ASL-CMR[1] and positron emission tomography studies.[40] MP measured during systole, however, was less variable across slices compared with MP measured during diastole. The variability across slices in estimated MP during diastole was within the ASL measurement variability.

4 | DISCUSSION

We present a careful analysis of SS-EPI for ASL-CMR and optimize its settings for 3T human MP imaging. We demonstrate that it provides equivalent measurements of MP compared with bSSFP, which is the current reference standard. We also demonstrate that its speed (~55 ms per image) enables sequential multi-slice imaging, which is a major step toward achieving whole-heart coverage with the duration of standard adenosine vasodilation (approximately 3 min).

An important feature of our SS-EPI implementation is the 2DRF pulse. This pulse enables the use of anrFOV for scan efficiency, while providing fat suppression, which is important because fat shifts along the phase-encode direction and can corrupt the ASL signal. This pulse also enabled sequential multi-slice imaging to improve spatial coverage of ASL-CMR, which is important because prior techniques for rFOV imaging were not compatible with both sequential multi-slice imaging, and fat suppression.[42]

Magnetization transfer (MT) effects of the proposed 2DRF SS EPI sequence were comparable to a standard SS-EPI spin echo sequence. The simulated MT ratio was 0.1%, 2.76%, and 5.46% for slices 1, 2, and 3, respectively.[43] The simulated MT ratio for slice 1 would result in a negligible loss in sensitivity and can be ignored. The effects for slices 2 and 3 are quite small compared with other sources of variability in ASL-CMR. Because the signal reduction will be identical for both control and label images, we expect this to slightly lower sensitivity (<6%) without introducing bias in MP measurements.

One limitation of the proposed 2DRF pulse is its sensitivity to off-resonance. The BW of the pulse in the slice-select direction was only 120 Hz. Shifts in the excitation profile could result in signal loss in the LV myocardium, because only the signal in pass-band of the 180-refocusing (BW ~1 kHz) pulse is refocused. The lateral wall of the myocardium typically experiences the highest off-resonance due to proximity to lungs and draining veins.[25] It is, therefore, most susceptible to signal loss from shifts in excitation profile. In this study, we mitigated this issue by setting the thickness of the 180°-refocusing pulse to 2× the imaging slice thickness. This provided tolerance to ±62.5 Hz off-resonance before experiencing any signal loss. The slice thickness of the refocusing pulse was not increased further to prevent refocusing fat signal that could also degrade image quality. This tradeoff in slice thickness of 180° pulse, off resonance sensitivity, and fat suppression warrants further study.

Another important feature of this study was the careful assessment of velocity selective saturation effects of the crusher gradients, specifically on myocardium and blood

pool signal. SS-EPI has previously been demonstrated for cardiac DTI[13] where the large motion sensitizing gradients provided blood pool suppression. Previous works have anecdotally demonstrated blood pool suppression using crusher gradients,[12] but did not systematically study the tradeoff between undesirable myocardial signal loss and desirable blood pool signal suppression based on the choice of V_c. We experimentally characterized myocardial signal loss in systolic and diastolic cardiac phases, and systematically arrived at the velocity cutoffs of 12.5 cm/s for diastole and 25 cm/s for systole. This study was performed in healthy volunteers and baseline images. Such a study may need to be carried on a larger cohort, including patients, for generality.

We demonstrate sequential multi-slice SS-EPI. A natural extension would be SMS SS-EPI, because of its higher SNR efficiency and even shorter acquisition duration. Previous works have demonstrated cardiac DTI imaging with SMS SS-EPI.[13] Lau et al used an acceleration factor of 3 ($R = 3$) to acquire slices simultaneously. We chose sequential multi-slice for an initial demonstration because it is compatible with all available cardiac coil geometries and does not require parallel imaging.

Systolic SS-EPI provided statistically equivalent MP measurements to reference diastolic 1RR bSSFP method, whereas MP was underestimated for systolic bSSFP. Systolic SS-EPI also had higher TSNR compared with systolic bSSFP. TSNR is used as a metric for measurement quality (sensitivity) of ASL. Therefore, these results indicate that SS-EPI provides more sensitive MP measurements during systole. The underestimation in MP and lower TSNR during systolic bSSFP may be due to motion artifacts, as shown in Figure 4. The imaging window in systolic bSSFP (~192ms) is longer than stable end-systole (80-100 ms @ heart rate of 60 beats per minute), which leads to us to expect substantial cardiac motion during the imaging window. SS-EPI has a much shorter imaging window (55 ms) with a readout duration of <25 ms and is, therefore, less susceptible to motion artifacts during systole or in subjects with higher heart rate.

We did not find MP in diastolic 2RR bSSFP to be equivalent to 1RR bSSFP at the difference level of 0.4 mL/g/min. Diastolic 1RR bSSFP was used as the reference method and 2RR bSSFP was acquired to perform a comparison with 2RR SS-EPI with 1º of variation. MP measured using diastolic and systolic SS-EPI was statistically equivalent to the reference method. MP measured using diastolic 2RR bSSFP was underestimated by approximately 20%. Bloch simulations with flow effects (not shown) suggest that an increase in PLD from 1RR to 2RR leads to roughly 5% underestimation of MP, due to partial labeling of the LV blood pool during control acquisitions that eventually reaches the target tissue. This may partially explain the observed underestimation.

We observed a difference in estimated MP and TSNR in lateral and septal myocardium using diastolic SS-EPI. Diastolic SS-EPI yielded MP values equivalent to both diastolic 1RR and 2RR bSSFP for the septal myocardium. In the lateral myocardium, however, MP was underestimated and TSNR was significantly lower for diastolic SS-EPI compared with diastolic bSSFP. The lower MP may be due to signal loss and the lower TSNR may also be due to an increase in PN. Lateral myocardium is more susceptible to both signal loss and PN due to (1) saturation effects of flow-suppressing crusher gradients because it moves at higher velocity than septal myocardium[44,45]; (2) off-resonance sensitivity of the 2DRF excitation profile, because it has higher off-resonance due to proximity to lungs and draining veins[25]; and (3) lower B1+, which causes lower signal due to both imperfect excitation and refocusing. Higher off-resonance in the lateral wall also causes geometric distortion, which can cause signal loss. All of these factors can vary with breath-holds and are an additional source PN. Significantly lower TSNR in the lateral myocardium is likely responsible for the lower TSNR of diastolic SS-EPI compared with diastolic bSSFP. Currently, diastolic bSSFP provides more sensitive MP measurements compared with diastolic SS-EPI, due to its higher TSNR. Improvements in SS-EPI image quality, especially in the lateral myocardium are needed to improve sensitivity of the technique.

SS-EPI images showed 2- to 3-fold variation in SNR across the myocardium where as bSSFP images showed only 1.5- to 2-fold variation. SNR variation in SS-EPI was higher likely due to (1) pile-up artifact from off-resonance, which can cause local signal enhancement; (2) B1+ sensitivity of both the excitation and refocusing RF pulses that can amplify the signal variation due to B1+; and (3) off-resonance sensitivity of the 2DRF pulse, which can cause signal loss. Pile up artifact from off-resonance can be reduced using parallel imaging. Composite pulses can be used to reduce the sensitivity of refocusing pulses to B1+ variations. These will be explored in future work to improve the image quality of SS-EPI at 3T.

MP measured for sequential multi-slice experiments showed very high variability for the apical slice acquired during diastole. This was likely due to poor image quality observed in diastolic apical slice due to poor blood pool suppression, and higher off-resonance.[25] We hypothesize that less blood is suppressed in the apical slice blood pool due to lower blood flow velocities,[46] and this blood pool signal can cause flow artifacts in SS-EPI images. This was not an issue for systolic imaging, because as shown in Figure 4, during end-systole blood pool is very small and myocardium is very thick for the apical slice. We did not experimentally evaluate the effect of slice acquisition order on image quality and MP quantification, and the apical slice was always acquired last. Therefore, slice acquisition order cannot be ruled out as a potential reason for high variability in the apical slice.

The MP quantification model used for myocardial ASL assumes constant flow during the cardiac cycle, which is an acceptable assumption when PLD is multiples of the RR interval. It yields average MP during the cardiac cycle. In sequential multi-slice ASL, PLD is a multiple of RR ±55 ms. The assumption of constant flow can cause a slight bias in MP quantification. The effect of this change is minimized by using a slice specific PLD. The residual error of the constant flow assumption is <5%, which is small compared with other sources of variability in ASL-CMR (~10-30%).

In multi-slice studies, we did not observe lower MP in slices that were further from the leading edge of the labeling slab in sequential multi-slice imaging. It has previously been hypothesized that transit delay sensitivity of FAIR ASL-CMR makes it incompatible with multi-slice imaging.[47] For both imaging during systole and diastole, this reduction in MP due to transit delay was not observed. This is likely due to the longer inversion time (2RR) used for SS-EPI ASL-CMR experiments, and the fact that all subjects were healthy.

Additionally, in multi-slice studies wide slice selective inversion slabs (70 mm and 50 mm) were used in the control acquisition. These will label large amounts of blood in the LV blood pool. This blood then perfuses the myocardium for the next few cardiac cycles (because ejection fraction is <100%), and will result in underestimation of MP. We performed Bloch simulations with flow effects (not shown for brevity), including the effect of partial labeling of LV blood pool. Underestimation is roughly 20% and 10% for diastolic and systolic imaging (PLD: 2RR), respectively. This underestimation is a significant limitation of the FAIR technique. This effect was not detected in the data, likely because variation in MP observed between subjects is >30%, which is large but consistent with previous ASL-CMR studies.[27,48] Larger sample sizes will be required to detect differences on the order of <30% with existing ASL-CMR techniques.

Our study had several limitations: (1) A small number of healthy volunteers were studied, and further validation in a larger population, including patients, will be valuable. (2) Segmental analysis to understand regional variability of multi-slice MP measurements was not performed in this study. Such analysis is very important for clinical use, and an in depth study of regional measurements, including their sensitivity to motion and partial voluming, will be valuable. (3) Reference acquisitions (DG-FAIR bSSFP) for multi-slice experiments were not acquired. Acquisition of such reference data would have made this experiment prohibitively long (several hours) for human volunteers. This would benefit from validation in large animals using reference CMR methods and/or gold standard measurements, such as microsphere. (4) Sensitivity of SS-EPI ASL-CMR measurements to V_c was not explored. We only explored the effect of V_c on SNR of LV myocardium and blood pool in baseline images. ASL-CMR is sensitive to <1% changes in image signal and future would should explore the effect of V_c on MP and TSNR. (5) Roughly 18% of data was rejected due to mistriggering, which we partially attribute to the use of plethysmograph. Electrocardiogram triggering could be used in future works to overcome this limitation.

5 | CONCLUSIONS

SS-EPI is an efficient acquisition scheme for ASL-CMR, with many benefits compared with bSSFP, including a shorter acquisition window and a simple multi-slice implementation. We have demonstrated SS-EPI with carefully optimized settings for human myocardial ASL-CMR at 3T during both systole and diastole. Single-slice MP measured using SS-EPI was statistically equivalent to diastolic bSSFP, which is the current reference method. We have also demonstrated sequential multi-slice imaging using SS-EPI for ASL-CMR without increasing in scan time.

ACKNOWLEDGMENTS

The authors also thank Hung P. Do, Terrence Jao, Nam Lee, and Vanessa Landes for helpful discussions during the course of the study. Preliminary versions of this work were presented at ISMRM 2017 (Abstract #3237), SCMR 2018 (Abstract #334), and ISMRM 2018 (Abstract #4240).

ORCID

Ahsan Javed https://orcid.org/0000-0003-1311-1247
Krishna S. Nayak https://orcid.org/0000-0001-5735-3550

TWITTER

Ahsan Javed @ahsan1237

REFERENCES

1. Zun Z, Wong EC, Nayak KS. Assessment of myocardial blood flow (MBF) in humans using arterial spin labeling (ASL): feasibility and noise analysis. *Magn Reson Med*. 2009;62:975–983.
2. Kober F, Jao T, Troalen T, Nayak KS. Myocardial arterial spin labeling. *J Cardiovasc Magn Reson*. 2016;18:22.
3. Lloyd-Jones D, Adams RJ, Brown TM, et al. Heart disease and stroke statistics - 2010 update: a report from the American heart association. *Circulation*. 2010;121:948–954.
4. Mozaffarian D, Benjamin EJ, Go AS, et al. Heart disease and stroke statistics-2016 update: a report from the American Heart Association. *Circulation*. 2016;133:e38–360.
5. Sieber MA, Lengsfeld P, Walter J, et al. Gadolinium-based contrast agents and their potential role in the pathogenesis of nephrogenic systemic fibrosis: the role of excess ligand. *J Magn Reson Imaging*. 2008;27:955–962.

6. United States Renal Data System. 2013 Atlas of CKD & ESRD. https://www.usrds.org/atlas13.aspx. Accessed December 24, 2019.
7. United States Renal Data System. Chapter 1: Incidence, Prevalence, Patient Characteristics, and Treatment Modalities. 2018. https://www.usrds.org/2018/download/v2_c01_IncPrev_18_usrds.pdf. Accessed December 24, 2019.
8. Epstein FH, Meyer CH. Myocardial perfusion using arterial spin labeling CMR. *JACC Cardiovasc Imaging*. 2011;4:1262–1264.
9. Cerqueira MD, Weissman NJ, Dilsizian V, et al. Standardized Myocardial Segmentation and Nomenclature for Tomographic Imaging of the Heart. *J Cardiovasc Magn Reson*. 2002;4:203–210.
10. Jao TR, Nayak K. Simultaneous Multi-slice Cardiac ASL. In: Proceedings of the 25th Annual Meeting of ISMRM, Honolulu, Hawaii, 2017. Abstract 1888.
11. Landes V, Jao T, Nayak K. Simultaneous multi-slice bSSFP CMR: is it feasible? In: SCMR 21st Scientific Session, Barcelona, Spain, 2018. Abstract 333.
12. Poncelet BP, Koelling TM, Schmidt CJ, et al. Measurement of human myocardial perfusion by double-gated flow alternating inversion recovery EPI. *Magn Reson Med*. 1999;41:510–519.
13. Lau AZ, Tunnicliffe EM, Frost R, Koopmans PJ, Tyler DJ, Robson MD. Accelerated human cardiac diffusion tensor imaging using simultaneous multislice imaging. *Magn Reson Med*. 2015;73:995–1004.
14. Ferreira PF, Kilner PJ, McGill L-A, et al. In vivo cardiovascular magnetic resonance diffusion tensor imaging shows evidence of abnormal myocardial laminar orientations and mobility in hypertrophic cardiomyopathy. *J Cardiovasc Magn Reson*. 2014;16:87.
15. Feinberg DA, Hoenninger JC, Crooks LE, Kaufman L, Watts JC, Arakawa M. Inner volume MR imaging: technical concepts and their application. *Radiology*. 1985;156:743–747.
16. Alley MT, Pauly JM, Sommer FG, Pelc NJ. Angiographic Imaging with 2D RF Pulses. *Magn Reson Med*. 1997;37:260–267.
17. Banerjee S, Nishimura DG, Shankaranarayanan A, Saritas EU. Reduced field-of-view DWI with robust fat suppression and unrestricted slice coverage using tilted 2DRF excitation: rFOV DWI with Tilted 2D RF Excitation. *Magn Reson Med*. 2016;76:1668–1676.
18. Pauly J, Le Roux P, Nishimura D, Macovski A. Parameter relations for the Shinnar-Le Roux selective excitation pulse design algorithm [NMR imaging]. *IEEE Trans Med Imaging*. 1991;10:53–65.
19. Conolly S, Nishimura D, Macovski A, Glover G. Variable-rate selective excitation. *J Magn Reson (1969)*. 1988;78:440–458.
20. Hargreaves BA, Cunningham CH, Nishimura DG, Conolly SM. Variable-rate selective excitation for rapid MRI sequences. *Magn Reson Med*. 2004;52:590–597.
21. Wong EC, Cronin M, Wu W-C, Inglis B, Frank LR, Liu TT. Velocity-selective arterial spin labeling. *Magn Reson Med*. 2006;55:1334–1341.
22. Wang J, Yarnykh VL, Hatsukami T, Chu B, Balu N, Yuan C. Improved suppression of plaque-mimicking artifacts in black-blood carotid atherosclerosis imaging using a multislice motion-sensitized driven-equilibrium (MSDE) turbo spin-echo (TSE) sequence. *Magn Reson Med*. 2007;58:973–981.
23. Jezzard P, Balaban RS. Correction for geometric distortion in echo planar images from B0 field variations. *Magn Reson Med*. 1995;34:65–73.
24. Schär M, Kozerke S, Fischer SE, Boesiger P. Cardiac SSFP imaging at 3 Tesla. *Magn Reson Med*. 2004;51:799–806.
25. Reeder SB, Faranesh AZ, Boxerman JL, McVeigh ER. In vivo measurement of T*2 and field inhomogeneity maps in the human heart at 1.5 T. *Magn Reson Med*. 1998;39:988–998.
26. Schenck JF. The role of magnetic susceptibility in magnetic resonance imaging: MRI magnetic compatibility of the first and second kinds. *Med Phys*. 1996;23:815–850.
27. Do HP, Yoon AJ, Fong MW, Saremi F, Barr ML, Nayak KS. Double-gated myocardial ASL perfusion imaging is robust to heart rate variation: double-gated myocardial ASL is robust to HRV. *Magn Reson Med*. 2017;77:1975–1980.
28. Uecker M, Lai P, Murphy MJ, et al. ESPIRiT-an eigenvalue approach to autocalibrating parallel MRI: where SENSE meets GRAPPA. *Magn Reson Med*. 2014;71:990–1001.
29. Roemer PB, Edelstein WA, Hayes CE, Souza SP, Mueller OM. The NMR phased array. *Magn Reson Med*. 1990;16:192–225.
30. Robson PM, Grant AK, Madhuranthakam AJ, Lattanzi R, Sodickson DK, McKenzie CA. Comprehensive quantification of signal-to-noise ratio and g-factor for image-based and k-space-based parallel imaging reconstructions. *Magn Reson Med*. 2008;60:895–907.
31. Javed A, Jao TR, Nayak KS. Motion correction facilitates the automation of cardiac ASL perfusion imaging. *J Cardiovasc Magn Reson*. 2015;17:1–2.
32. Avants B, Tustison N, Song G. Advanced normalization tools (ANTS). *Insight J*. 2009;1–35.
33. Jao T, Zun Z, Varadarajan P, Pai R, Nayak K. Spatiotemporal filtering of myocardial ASL data: implications in detection and diagnosis of coronary artery disease. In: Proceedings of the 20th Annual Meeting of ISMRM, Melbourne, Australia, 2012. Abstract 3892.
34. Kellman P, Hansen MS. T1-mapping in the heart: accuracy and precision. *J Cardiovasc Magn Reson*. 2014;16:2.
35. Buxton RB, Frank LR, Wong EC, Siewert B, Warach S, Edelman RR. A general kinetic model for quantitative perfusion imaging with arterial spin labeling. *Magn Reson Med*. 1998;40:383–396.
36. Weingärtner S, Meßner NM, Budjan J, et al. Myocardial T1-mapping at 3T using saturation-recovery: reference values, precision and comparison with MOLLI. *J Cardiovasc Magn Reson*. 2017;18:84.
37. Cerqueira MD, Weissman NJ, Dilsizian V, et al. Standardized myocardial segmentation and nomenclature for tomographic imaging of the heart. *Circulation*. 2002;105:539–542.
38. Walker E, Nowacki AS. Understanding equivalence and noninferiority testing. *J Gen Intern Med*. 2011;26:192–196.
39. Zaglavara T, Haaverstad R, Cumberledge B, et al. Dobutamine stress echocardiography for the detection of myocardial viability in patients with left ventricular dysfunction taking β blockers: accuracy and optimal dose. *Heart*. 87:329–335.
40. Chareonthaitawee P. Heterogeneity of resting and hyperemic myocardial blood flow in healthy humans. *Cardiovas Res*. 2001;50:151–161.
41. Motwani M, Kidambi A, Uddin A, Sourbron S, Greenwood JP, Plein S. Quantification of myocardial blood flow with cardiovascular magnetic resonance throughout the cardiac cycle. *J Cardiovasc Magn Res*. 2015;17:4.
42. Wargo CJ, Moore J, Gore JC. A comparison and evaluation of reduced-FOV methods for multi-slice 7T human imaging. *Magn Reson Imaging*. 2013;31:1349–1359.
43. Gloor M, Scheffler K, Bieri O. Quantitative magnetization transfer imaging using balanced SSFP. *Magn Reson Med*. 2008;60:691–700.
44. Codreanu I, Robson MD, Golding SJ, Jung BA, Clarke K, Holloway CJ. Longitudinally and circumferentially directed movements of the left ventricle studied by cardiovascular magnetic resonance phase contrast velocity mapping. *J Cardiovasc Magn Reson*. 2010;12:48.

45. Greaves K, Puranik R, O'Leary JJ, Celermajer DS. Myocardial tissue velocities in the normal left and right ventricle: relationships and predictors. *Heart Lung Circ*. 2004;13:367–373.
46. Buchenberg WB, Markl M, Bauer S, Bock J, Lorenz R, Jung BA. Dual VENC phase contrast MRI for simultaneous assessment of blood flow and cardiac motion. In: Proceedings of the 19th Annual Meeting of ISMRM, Montréal, 2011. Abstract 3303.
47. Jao TR, Nayak KS. Demonstration of velocity selective myocardial arterial spin labeling perfusion imaging in humans: demonstration of velocity selective myocardial arterial spin labeling perfusion imaging in humans. *Magn Reson Med*. 2018;80:272–278.
48. Zun Z, Varadarajan P, Pai RG, Wong EC, Nayak KS. Arterial spin labeled CMR detects clinically relevant increase in myocardial blood flow with vasodilation. *JACC Cardiovasc Imaging*. 2011;4:1253–1261.

SUPPORTING INFORMATION

Additional supporting information may be found online in the Supporting Information section.

FIGURE S1 Scatter plot of normalized signal from all segments and all subjects plotted. There was no detectable saturation of myocardium using the SS-EPI sequence, using V_c ≥12cm/s for diastolic and ≥25 cm/s for systolic

FIGURE S2 Bullseye plots showing estimated velocities for 3 subjects. The average velocity during stable diastole is estimated to be 0.3-1.6 cm/s across subjects. The average velocity during stable systole is estimated to be 0.9 – 4.3 cm/s. In general, the residue was low and about the same throughout the myocardium, indicating goodness of fit for this simple model. Additionally, myocardial velocity during systole was slightly higher in the lateral wall compared to the septal wall, consistent with the literature (4)

FIGURE S3 Six segment measured data (dots) and fitted data (solid line) for a representative subject during diastole and systole. Increasing velocity cutoff increased the signal in diastole and systole. Also shown are representative images demonstrating the change in SNR with Vc. Qualitatively, this also helps verify the difference in cardiac wall motion as predicted by the velocity maps shown in the Fig. S2 (i.e. the cardiac velocity is slightly higher in the lateral wall than the septal wall)

How to cite this article: Javed A, Nayak KS. Single-shot EPI for ASL-CMR. *Magn Reson Med*. 2020;84:738–750. https://doi.org/10.1002/mrm.28165